Bioelectrochemistry 147 (2022) 108197

Contents lists available at ScienceDirect

Bioelectrochemistry

journal homepage: www.journals.elsevier.com/bioelectrochemistry

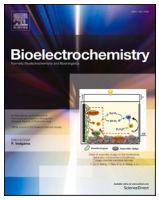

Microtrap array on a chip for localized electroporation and electro-gene transfection

Aswin Muralidharan [a,*,1,2], Georg R. Pesch [a,1,3], Hendrik Hubbe [a], Lea Rems [b], Mahdiyeh Nouri-Goushki [a], Pouyan E. Boukany [a,*]

[a] Department of Chemical Engineering, Delft University of Technology, van der Maasweg 9, 2629 HZ Delft, the Netherlands
[b] Faculty of Electrical Engineering, University of Ljubljana, Trzaska 25, 1000 Ljubljana, Slovenia

ARTICLE INFO

Keywords:
Localized electroporation
Electrotransfection
Microfluidics
Gene delivery

MSC[2010]:
00–01
99–00

ABSTRACT

We developed a localized single-cell electroporation chip to deliver exogenous biomolecules with high efficiency while maintaining high cell viability. In our microfluidic device, the cells are trapped in a microtrap array by flow, after which target molecules are supplied to the device and electrotransferred to the cells under electric pulses. The system provides the ability to monitor the electrotransfer of exogenous biomolecules in real time. We reveal through numerical simulations that localized electroporation is the mechanism of permeabilization in the microtrap array electroporation device. We demonstrate the simplicity and accuracy of this microtrap technology for electroporation by delivery of both small molecules using propidium iodide and large molecules using plasmid DNA for gene expression, illustrating the potential of this minimally invasive method to be widely used for precise intracellular delivery purposes (from bioprocess engineering to therapeutic applications).

1. Introduction

Precise intracellular biomolecule delivery in a safe, affordable, and robust way is key to fundamental cell biology research and biomedical applications. Transient permeabilization of cell membranes using pulsed electric fields (electroporation) is a simple non-viral method to deliver exogenous biomolecules to a variety of cell types [1–6]. However, conventional electroporation often suffers from poor efficiency as it relies on bulk stochastic phenomena and poor control over the cell viability due to the strong electric fields used [7,8].

To obtain non-toxic electroporation with controlled biomolecule delivery, it is required to apply electric pulses through miniaturized (small) geometries, which induce localized electroporation at the cell membrane [9–12]. In localized electroporation, the applied electric field is concentrated by utilizing miniaturized structures such as micro/nanochannels [9,13–23], porous membranes [10,24], nanostraws [25–27], nanotubes [28], nanoprobes [29–31], or microneedles [32–34]. This can provide precise control over the dosage of the delivered exogenous cargo [9,10]. Localized electroporation is compatible with delivering a variety of exogenous cargo such as molecular beacons [9,35], lipoplex nanoparticles [36], siRNA [37], mRNA [10], plasmid DNA [9,10,22,24], and Cas9 ribonuclear proteins [10] while maintaining high cell viability. However, the cells should either be adhered to the structures (or substrate) [10,22,26] or be micromanipulated to the structure through an external force (e.g., by optical and magnetic tweezers or a micromanipulator) [9,31] for successful localized electroporation.

To overcome this limitation, we fabricated a scalable hydrodynamic microtrap array integrated into a microfluidic channel [38,39] (or microtraps for brevity) to simultaneously immobilize cells at miniaturized constrictions and perform localized electroporation. The cells are trapped in the microtraps through flow and are tightly attached to the trap's aperture, where the applied voltage drop in the channel is concentrated. Our device enables us to electroporate single trapped cells while maintaining high cell viability (> 90%) and deliver small biomolecules and plasmid DNA encoding functional proteins. The cells can

* Corresponding authors.
E-mail addresses: a.muralidharan@tudelft.nl (A. Muralidharan), p.e.boukany@tudelft.nl (P.E. Boukany).
[1] These authors contributed equally to this work.
[2] Present address: Department of Bionanoscience, Kavli Institute of Nanoscience, Delft University of Technology, van der Maasweg 9, 2629 HZ Delft, the Netherlands.
[3] Present address: University of Bremen, Faculty of Production Engineering, Chemical Process Engineering, Leobener Strasse 6, 28359 Bremen, Germany.

https://doi.org/10.1016/j.bioelechem.2022.108197
Received 1 March 2022; Received in revised form 9 June 2022; Accepted 25 June 2022
Available online 28 June 2022

be continuously perfused with the culture media required for maintaining cell viability. We further confirm through numerical calculations that our device enables localized electroporation, with enhanced electroporation at the cell region facing the microtrap aperture and reduced electroporation in the remainder of the cell. Our microtrap electroporation device is a demonstration of a microfluidics approach, wherein single-cell trapping (under gentle flow conditions) and electrical pulses control the precise delivery of cargo into the cell. This microtrap localized electroporation device is anticipated to provide new opportunities for accurate and efficient drug delivery, *ex vivo* and gene editing application in cell biology and medicine.

2. Materials and methods

2.1. Cell culture and preparation for microtrap electroporation

The Chinese Hamster Ovary cells, CHO-K1 (DSMZ), are routinely cultured in T25 flasks containing 5 ml culture medium consisting of Nutrient Mixture Ham's F-12 (Sigma Aldrich) supplemented with ~ 10% Fetal Bovine Serum (Sigma Aldrich). When the cells attain ~ 80 −100% confluency, 1 µl of 5 mM Calcein AM or Calcein Red AM (both AAT Bioquest) is added to the T25 flasks to fluorescently label the cells for ease of visualization (final Calcein AM concentration ~ 1 µM). After incubating the cells with Calcein AM for 15–25 min in the incubator, cells are harvested by treating with trypsin–EDTA 0.25% (Sigma Aldrich). The cell-trypsin suspension is diluted with 5 ml Opti-MEM serum-free medium (Gibco) and then centrifuged. The supernatant is removed, and the cell pellet is suspended in 45 ml Opti-MEM serum-free medium to transfer to the microtrap electroporation device.

2.2. Preparation of fluorescent molecules and plasmids for assessment of electroporation

Propidium iodide (PI), a membrane impermeant nucleic acid fluorescent stain, is used to assess the microtrap array electroporation efficacy. The stock solution of PI was diluted to 25 µM in Opti-MEM before electroporation experiments. PI binds to nucleic acids and emits a strong fluorescence signal with an excitation/emission wavelength of 535/615 nm upon successful membrane permeabilization. We pre-stain the CHO cells with Calcein AM with an excitation/emission wavelength of 488/520 nm for PI delivery experiments. The pre-staining of CHO cells with Calcein AM provides a more precise visualization and tracking of the trapped cells inside the microfluidic chip.

To assess the microtrap array electro-gene transfection efficacy, pEGFP-C1 plasmid DNA is used. To prepare the plasmids for electro-gene transfection, DH5α *E. coli* cultures are transformed with the pEGFP-C1 plasmids using heat shock. The plasmids are then extracted and purified using the GeneJET Plasmid Miniprep Kit. The DNA solution is diluted to 20 µg/ml in Opti-MEM for microtrap electro-gene transfection experiments. Upon successful transfection, the pEGFP-C1 plasmids express a green fluorescent protein (GFP) with an excitation/emission wavelength of 488/507 nm. We pre-stain the cells with Calcein Red AM with an excitation/emission wavelength of 560/574 nm for the electro-gene transfection experiments.

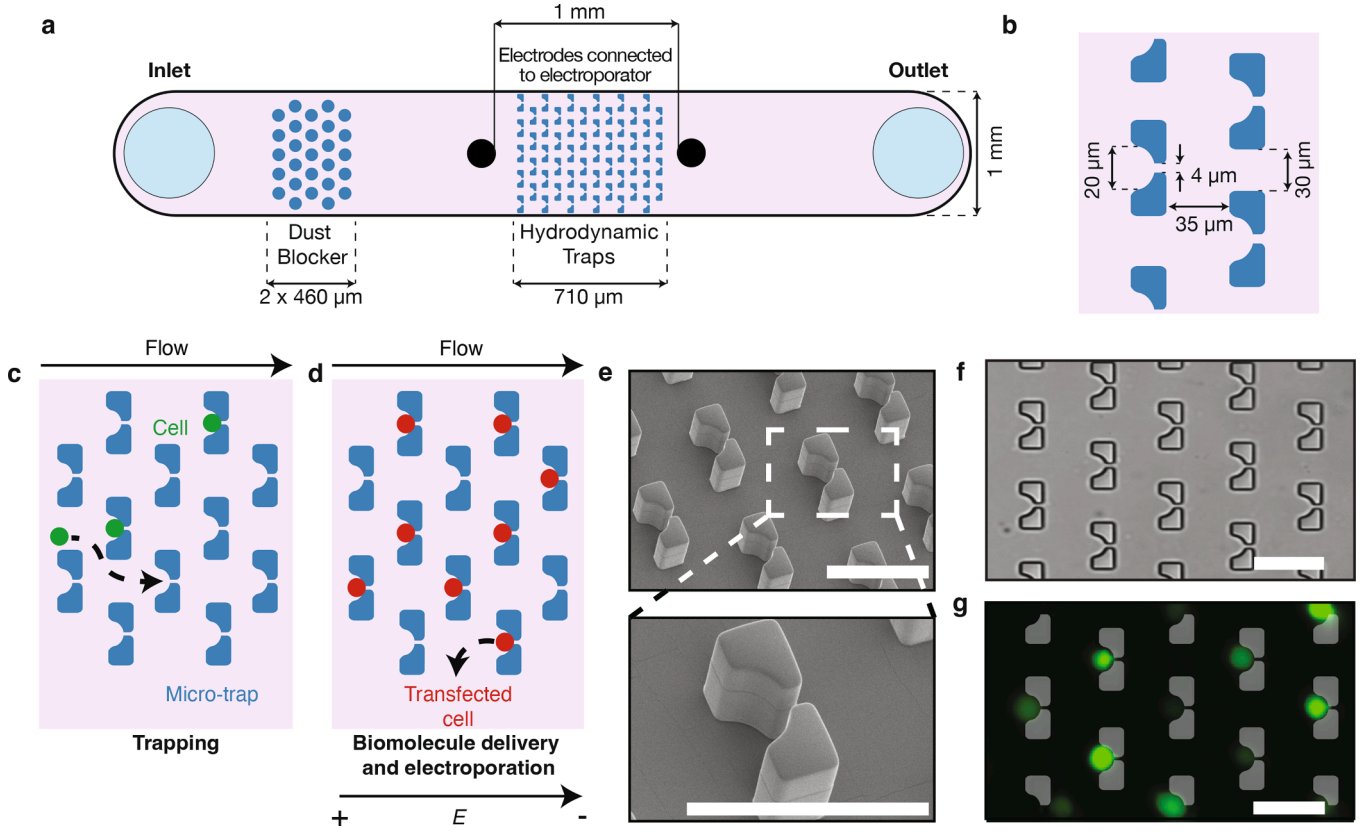

Fig. 1. Microtrap array on a chip for localized electroporation working principle and design. (a) Schematic representation of the overall setup. Relevant dimensions are denoted in the figure. The fabricated PDMS device consists of two sets of dust blockers to remove large debris near the inlet, a 710 µm long array of microtraps, and two electrodes separated by 1 mm. The device is 35 µm high. (b) The relevant dimensions of the microtraps are provided in this schematic. (c)-(d) Working principle of microtrap electroporation; (c) Stage 1: Hydrodynamic trapping of the cells in the microtraps by flowing cell suspension using a syringe pump, (d) stage 2: biomolecules are then delivered as a solution with a syringe pump to the microchannel and then delivered to the cells by application of electric fields. (e) Scanning electron microscopy images of the PDMS device (bottom is the zoomed in view of a single trap) containing the microtraps. (f) Brightfield image showing traps in the microfluidic device without the cells. (g) Calcein stained cells (stained for better clarity during visualization) have been trapped in the microtrap array. Scale bar is 50 µm.

2.3. Device fabrication and experimental setup

To perform microtrap localized electroporation, we designed a device with the following working principle. Single cells supplied to the device should be trapped in the microtraps until the streamlines through the trap aperture are closed, as displayed in Fig. 1(c). The applied electric field electroporates the cells trapped in the array. The field is locally amplified in the trap aperture caused by the insulating polydimethylsiloxane (PDMS) constriction. This enables localized electroporation and controlled transfer of cell membrane impermeant (bio-) molecules to cells, as displayed in Fig. 1(d).

The microchannels for microtrap array electroporation with the above requirements are fabricated from PDMS (Dow Sylgard 184) using standard soft lithography procedure [40]. The micro master mold is created in silicon using electron-beam lithography and novolac-based resist to pattern a plasma-enhanced chemical vapor deposition (PECVD) SiO_2 hard mask, followed by fluorine-based dry etching of the hard mask and Bosch process deep reactive-ion etching (DRIE) of the silicon to a depth of 35 μm. The microfluidic patterns are transferred from the micro mold to a PDMS block and then cured overnight after mixing with Dow Sylgard 184 curing agent (PDMS to curing agent mixing ratio is 10:1) in the oven at 68 °C. The PDMS device consists of two sets of dust blockers near the inlet and a microtrap array containing 203 traps, each with a trap aperture of 4 μm. Four openings are punched into the PDMS block using biopsy punches for the device's inlet and outlet (diameter 1.5 mm) and two electrodes (diameter 0.5 mm). A glass slide spin-coated with a thin layer of PDMS is used to seal the microfluidic device after treating both the top and bottom surfaces with air plasma (Harrick Plasma PDC-002). The assembled microfluidic device is then cured in the oven for 12 h at 68 °C. The fabricated PDMS device and the structures are characterized after gold sputtering for 60 s (with JEOL JFC-1300 auto fine coater) on the PDMS device with a scanning electron microscope (JEOL JSM-2010LA) as shown in Fig. 1(e). Fig. 1(f) displays a section of the microtrap array (brightfield microscopy image) before trapping the cells. Fig. 1(g) shows an example of trapped calcein-stained CHO cells (shown in green).

2.4. Delivery of biomolecules using microtrap array electroporation

To handle the samples (pre-stained cell suspension, pure Opti-MEM, and fluorescent molecules or plasmids), the required solutions are collected in 5 ml syringes. All the solutions are supplied using syringe pumps (Harvard Apparatus Pump 11 Elite). A 4-way IDEX valve connects the syringes to the microfluidic chip through polytetrafluoroethylene tubing (Kinesis, OD/ID 1.6 mm/0.8 mm). The 4-way connection to the valve is as follows: *(i)* input cell suspension or the target molecule solution, *(ii)* pure OptiMEM solution, *(iii)* inlet to the microtrap array device, *(iv)* waste. Two 0.5 mm platinum wires are used as electrodes and are connected before and after the microtrap array (spaced approximately 1 mm apart). The platinum wires are connected to a pulse generator (BETA tech Electrocell S20) to deliver the electric pulses. Once the required connections are inserted, the microtrap array device is flushed with pure Opti-MEM (flow rate = 50 ml/h or 833 μl/min) to remove the air in the system. Once the system is free of air, the pre-stained cell suspension is added to the microtrap array device at a flow rate of 50 μl/min by switching the IDEX valve. When the cells trap inside the microtraps, the flow rate is reduced to 10 μl/min for 10 min. Then, the IDEX valve is switched back to pure Opti-MEM supply at 10 μl/min. Reduction in flow rate maintains the pressure on the cells but avoids uncontrolled cell accumulation. The input syringe containing cell suspension is then replaced by the syringe containing the target molecule, which is supplied at a flow rate of 10 μl/min. The IDEX valve is now switched again so that the target biomolecule is supplied to the microtrap array device for 10 min. The flow is then stopped and the appropriate electric pulses are applied. Opti-MEM supplemented with 20% FBS is supplied to the microtrap array device at a flow rate of 0.01 μl/min after the electric pulses are delivered during the electro-gene transfection experiments. This allowed us to maintain cell viability for longer than 24 h.

2.5. Fluorescence imaging of molecular uptake during microtrap array electroporation

To visualize the uptake of fluorescent molecules and GFP expression, we use an inverted fluorescent microscope (Zeiss Axio-Observer) equipped with a 10× objective (Zeiss Plan-Apochromat 10 × /0.45 M27). This provides a field of view corresponding to ~$1.29 \times 1.29\ mm^2$. A light-emitting diode (LED) light source (Zeiss Colibri 7) is used with appropriate single bandpass filters for fluorescence imaging. The images are acquired using an Orca Flash 4.0 V2 (Hamamatsu) digital camera with a resolution of $2048 \times 2048\ px^2$ at the following frame rates: *(i)* the propidium iodide uptake experiments are imaged at 2 Hz, and *(ii)* the GFP expression in the cells is monitored by imaging at one frame per hour with an excitation/emission wavelength of 488/507 nm. The propidium iodide uptake and cell viability experiments are performed in triplicate at each voltage. The GFP expression experiments are done once at each voltage.

2.6. Numerical simulation of microtrap electroporation

To calculate the electric potential (V) distribution in the intracellular and extracellular space, the Laplace equation,

$$\nabla\left[\frac{\partial \epsilon_{i,e}\nabla V}{\partial t} + \left(\sigma_{i,e}\right)\nabla V\right] = 0 \tag{1}$$

is solved using COMSOL Multiphysics 5.6 as a 3D time-dependent model. To minimize computational cost, we simulate one unit cell of the periodic array of traps with cells. σ is the electric conductivity, ϵ is the dielectric permittivity of the intracellular (subscript i) and extracellular (subscript e) medium. The cell membrane is modeled via a distributed impedance boundary condition

$$\mathbf{n}\cdot\mathbf{J} = \frac{\sigma_m}{d_m}\left(V_i - V_e\right) + \frac{\epsilon_m}{d_m}\left(\frac{\partial V_i}{\partial t} - \frac{\partial V_e}{\partial t}\right) \tag{2}$$

where $\mathbf{n}$ is the unit vector normal to the membrane surface, $\mathbf{J}$ is the electric current density across the membrane, where as σ_m, ϵ_m, d_m denote the membrane conductivity, dielectric permittivity and thickness respectively [41]. V_i and V_e are the electric potential on the interior side and the exterior side of the cell membrane respectively. The transmembrane voltage V_m corresponds to the difference between the electric potentials on the two sides of the membrane ($V_m = V_i - V_e$) (see Table 1 for details of the parameters used for performing numerical simulations).

Table 1
Parameters used for the numerical simulations in this study.

Parameter	Value	Description
σ_{PDMS}	4×10^{-13} S/m	PDMS conductivity
ϵ_{PDMS}	2.75	PDMS permittivity
σ_e	1.5 S/m	Extracellular conductivity
ϵ_e	80	Extracellular permittivity
σ_i	0.5 S/m	Intracellular conductivity
ϵ_i	80	Intracellular permittivity
ϵ_m	5	Cell membrane permittivity
σ_m	3×10^{-7} S/m	Cell membrane conductivity
V_{ep}	0.258 V	Threshold electroporation voltage
α	1×10^{9} $m^{-2}s^{-1}$	Electroporation parameter
N_0	1.5×10^{9} m^{-2}	Equilibrium pore density when $V_m = 0$ V
q	2.46	Electroporation constant
r_p	1×10^{-9} m	Pore radius
d_m	5×10^{-9} m	Membrane thickness
r	10×10^{-6} m	Cell radius

To numerically describe electroporation, we use the asymptotic model of electroporation [42–45]. The model describes the rate of formation of transient hydrophilic pores in the cell membrane, which are permeant to ions and molecules as a function of V_m. According to the model, hydrophilic pores nucleate in the cell membrane at an initial radius r_p at a rate described by

$$\frac{dN}{dt} = \alpha e^{\left(\frac{V_m}{V_{ep}}\right)^2}\left(1 - \frac{N}{N_0} e^{-q\left(\frac{V_m}{V_{ep}}\right)^2}\right) \tag{3}$$

where N is the membrane pore density, N_0 is the pore density in the non-electroporated membrane, and α, q, and V_{ep} are electroporation parameters. Once the cell membrane is porated, the cell membrane conductivity is described as

$$\sigma_{ep} = \frac{2\pi r_p^2 \sigma_p d_m N}{(\pi r_p + 2d_m)} \tag{4}$$

where the conductance of single pore $\sigma_p = (\sigma_e - \sigma_i)/\log(\sigma_e/\sigma_i)$ and r_p is the radius of a single pore [45]. Membrane conductivity σ_m is thus the sum of the passive membrane conductivity σ_{cm} and σ_{ep}. Eqs. (1)–(4) were solved simultaneously with a linear system solver MUMPS. The numerical models and AutoCAD designs used in this study are publicly available on GitHub (https://github.com/aswinmuralidharan/Microtrap-Electroporation).

3. Results and discussions

3.1. Microtrap array electroporation has high electroporation efficiency and maintains high cell viability

To investigate the effect of PDMS microtraps on the applied voltage, the electric potential distribution in the microchannel is estimated by solving the steady-state version of the Eq. (1) in a two-dimensional space using COMSOL Multiphysics, where σ is the conductivity, and ϵ is the dielectric permittivity of the extracellular medium. The geometry of the device used for numerical simulations is in accordance with the chip used in the microtrap electroporation experiments (see supplementary information Fig. S1). To visualize the electric field amplification provided by the PDMS pillars in the microtrap array, we introduce the electric field amplification factor, defined as E/E_{-traps}, where E is the local electric field and E_{-traps} is the electric field in the absence of traps, defined as the ratio of the applied voltage to the distance between conventional parallel plate electrodes. The amplification factor shown in Fig. 2(a). Fig. 2(a) demonstrates that the electric field is amplified approximately three times at the aperture of the microtrap. This means, at the center of the trap aperture, the electric field can get as high as 225

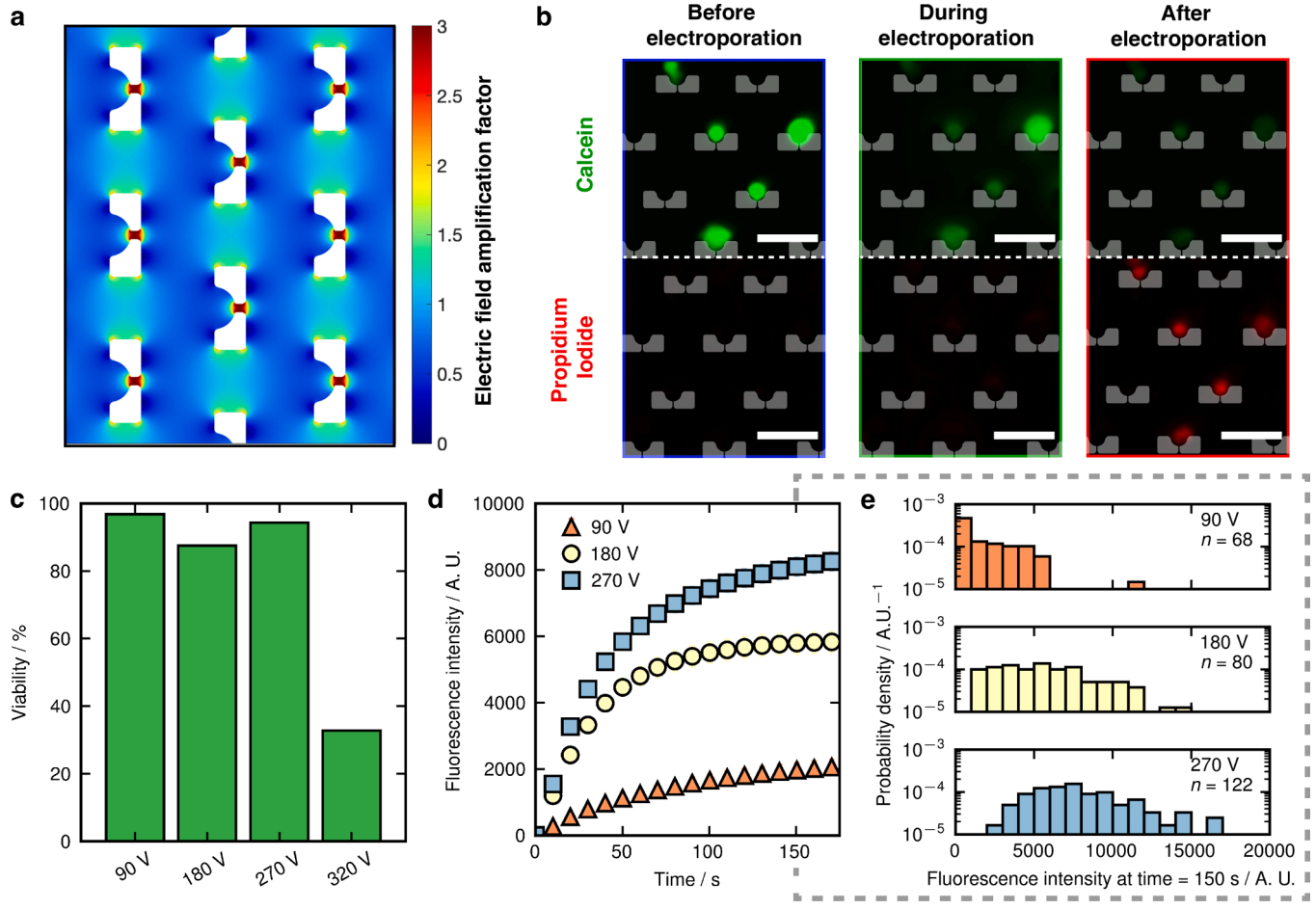

Fig. 2. Influence of the microtrap array on the electric field, molecular uptake and cell viability. (a) Electric field distribution in the microfluidic device shows locally amplified electric fields near the traps enabling localized electroporation. The electric field distribution in the region of the PDMS microtrap array is not displayed for ease of visualization. (b) *Top:* Efflux of Calcein before electroporation (left), during electroporation (middle), and after electroporation (right). *Bottom:* Uptake of propidium iodide before electroporation (left), during electroporation (middle), and after electroporation (right) is shown. (c) Cell viability for different applied voltages is plotted. (d) Average fluorescence intensity of propidium iodide uptake from several cells (number of cells $n = 68$ for 90 V, 80 for 180 V and 122 for 270 V) is plotted against time for different applied voltages. Raw data is provided in the supplementary information, Fig. S4. (e) Histogram (bin size = 1000 A.U.) of propidium iodide fluorescence intensity at 150 s showing the cell-to-cell variability in the uptake of propidium iodide. Scale bar is 50 μm.

V/mm and 810 V/mm for an applied voltage-to-distance ratio of 90 V/mm and 320 V/mm respectively (detailed figures are presented in the supplementary information, Fig. S2 and S3). Furthermore, electric fields in each trap are identical, allowing us to perform electroporation of cells at high throughput, with all cells exposed to similar electric fields. The needle electrode configuration does not change the calculated electric field distribution considerably due to the high resistance of the microtrap array (see supplementary information, Fig. S9).

To determine which operating voltages provide reversible electroporation conditions in the microtrap array, we experimentally investigate the influence of the applied voltage on the cell viability and small molecule electrotransfer to CHO-K1 cells. To do so, we trapped Calcein AM (green) stained CHO-K1 cells in the microtrap array and applied single electric pulses with voltages ranging from 90 V to 320 V with a pulse duration of 5 ms. When the cells are electroporated, the Calcein is rapidly expelled from the cells through the electropermeabilized cell membrane as shown in Fig. 2(b, top row). The electropermeabilized cell membrane is then allowed to recover for 1 h. One hour after applying electric pulses, a solution of Calcein Red AM (red) in Opti-MEM is supplied to the microchannel for 20 min. The channels are then flushed with Opti-MEM to remove any residual Calcein Red AM. Calcein Red AM is cell membrane permeable and is cleaved by live cells to form fluorescent Calcein molecules, which allows us to estimate the number of live cells after electroporation. We count the number of cells exhibiting red fluorescence to calculate the percentage of viable cells. We estimate between $>$ 90 % cell viability for applied voltages between 90 V and 270 V, followed by a sharp decrease to $\sim$ 30 % cell viability at 320 V as shown in Fig. 2(c). Hence, we set our operating voltage range for molecular delivery with reversible electroporation between 90 V and 270 V.

3.2. Analysis of small molecules uptake with microtrap array electroporation

To study the small molecule electrotransfer to the cell in the microtrap array on a chip, we monitor the electrotransfer of propidium iodide to CHO-K1 cells as a response to a single 5 ms long electric pulse of various applied voltages (90 V to 270 V) *in situ* using an inverted fluorescence microscope. Propidium ions are cell membrane impermeant and emit a strong fluorescence (excitation/emission 535 nm/615 nm) upon entry to a cell by binding to the nucleic acids present inside the cell [46–48]. The enhancement in propidium fluorescence intensity can hence be used as a marker for cell membrane permeabilization as a response to electric pulses, as shown in Fig. 2(b) (bottom panels). Fig. 2 (d) shows that propidium ions enter the cells at voltages from 90 V (lower voltages were not tested). We observe nearly 100% of the cells become permeable to propidium ions upon electroporation in the tested conditions. Suppose τ is the resealing time of the cell membrane, A_{p0} is the initial electropermeabilized area, d_m is the thickness of the cell membrane, D is the diffusion coefficient of propidium ions in the electroporation buffer, V is the volume of the cell, and c_e is the extracellular propidium concentration. Then, the concentration of bound propidium ions which emit the fluorescence at time t can be expressed as [46,48,49].

$$[\mathrm{PIB}] = \frac{Dc_e A_{p0}\tau}{Vd_m}(1 - \exp(-t/\tau)). \quad (5)$$

To assess the influence of applied voltage on the cell resealing time during microtrap electroporation, we extracted the resealing time τ and $I_{max} = Dc_e A_{p0}\tau/Vd_m$ by fitting the bound propidium fluorescence intensity time series with Eq. (5). We observe that the highest resealing time is for the lowest tested voltage (90 V) ($\sim 62 \pm 4$ s). At higher voltages, we observe lower resealing times ($\sim 35 \pm 2$ s for 180 V and $\sim 42 \pm 2$ s for 270 V). The distribution of fluorescence intensity in the electrotransferred cells at time $t = 150$ s after electrotransfer (i.e., a time point long after the resealing time) is plotted in Fig. 2(e). Since the time scale of molecular uptake is much greater than the duration of the electric pulse, post-pulse diffusion is the driving force for the molecular uptake for the small molecule electrotransfer in the microtrap array electroporation [46]. The mean propidium fluorescence intensity shifts to higher values with increasing applied voltages, implying that more molecules are electrotransferred at higher voltages despite lower resealing times (see Fig. S5). This means that there is a higher degree of electroporation at higher applied voltages. We then extract $I_{max}/\tau = Dc_e A_{p0}/Vd_m$ to estimate the increase in permeabilized area for different applied voltages. We estimate that $I_{max}/\tau = 69 \pm 28\ s^{-1}$ for 90 V, $208 \pm 16\ s^{-1}$ for 180 V, and $298 \pm 34\ s^{-1}$ for 270 V. Since all the parameters in the definition of I_{max}/τ except the initial permeabilized area are independent of applied voltage, this means that there is ~ 4.3 times more porated area at 270 V compared to 90 V in the microtrap electroporation.

We then compare the effectiveness of the microtrap electroporation to the bulk electroporation. To do so, we plate Calcein-stained CHO cells suspended in cell culture media on four well-chambered glass slides 1 h prior to applying electric pulses. The cell culture media is replaced with Opti-MEM, which contains the same concentration of PI (25 μM) as in microtrap electroporation. The electric pulses are applied through stainless steel electrodes placed parallel to each other and separated by a distance of 3 mm connected to the same pulse generator used for the microtrap electroporation system. We then apply a single 5 ms pulse of 270 V (comparable to the situation in microtrap electroporation with a voltage drop of 90 V since the electrodes in bulk electroporation are separated by 3 mm while in microtrap electroporation are separated by 1 mm). In contrast to microtrap electroporation, we observe minimal uptake of PI, which shows that the microtrap electroporation device is more effective in electroporating CHO cells than bulk electroporation. We analyze PI uptake from 280 cells and observed that the fluorescence intensity of the cells 150 s after bulk electroporation was 251 ± 12 A.U. (see supplementary information Fig. S6), while in microtrap electroporation under the same conditions, it was 1948 ± 248 A.U. Since the PI fluorescence signal after bulk electroporation provide a poor signal to noise ratio, we could not extract the fitting parameters using the Eq. (5). These results demonstrate that microtrap electroporation is more effective in electroporating and transferring exogenous biomolecules than bulk electroporation.

3.3. Microtrap array electroporation induces localized cell membrane electroporation

To investigate how the application of electric fields across the microtrap array provides a high degree of electroporation, we performed numerical simulations of electroporation using the asymptotic model of electroporation [44] (for the simulation geometry, see supplementary information, Fig. S10). To test the validity of the numerical solutions, we first estimated the electric field distribution and induced transmembrane voltage of an isolated cell in a homogeneous electric field without the pore formation equations. We show that our numerical solution agrees well with the analytical solution for the induced transmembrane voltage, $V_m = 1.5Er\cos\theta(1 - \exp(-t/\tau_m))$ [50] (see supplementary information, Fig. S7). Here, r is the radius of the cell, τ_m is the membrane charging time, E is the electric field, and θ is the angle measured from the center of the cell with respect to the direction of the electric field. To estimate which voltage drop to apply across each unit cell in our simulation, we measured the voltage drop across a unit cell of width 48.8 μm (see supplementary information, Fig. S8) from the 2D model discussed in the previous section. An applied voltage difference of 90 V, 180 V, and 270 V across electrodes in the experiment corresponds to a voltage drop of 3.6 V, 7.36 V, and 11.05 V across the simulation unit cell. One electrode was excited by a 5 ms rectangular pulse of the amplitude corresponding to this measured voltage drop by subtracting

two Heaviside step functions. The second electrode was set to ground.

Having established that our numerical solutions capture the induced transmembrane voltage without poration well, we then include the pore formation equations in the model. Fig. 3(a) shows that the presence of the microtrap alters the induced transmembrane voltage. The high induced transmembrane voltage regions are localized near the microtrap aperture in microtrap array electroporation than bulk electroporation (see supplementary information, Fig. S11). As a consequence of the high local induced transmembrane voltage, microtrap electroporation can lead to two to three times greater local pore area density near the trap aperture compared to the bulk electroporation, as shown in Fig. 3(b), (c). Besides the local amplification of pore formation near the trap aperture, the rest of the cell membrane display diminished pore formation as we show in Fig. 3(c). As a result, at 90 V, the average pore area density is comparable in both microtrap and bulk electroporation. Fig. 3(d) shows that microtrap electroporation at 180 V and 270 V leads to $\sim$ 40% higher pore area density than bulk electroporation and has over three times higher pore area density near the trap aperture. Deformation of the cells in the trap aperture shows no appreciable increase in pore area density (see supplementary information, Fig. S12).

Our numerical simulations show that the high efficiency of electroporation in the microtrap electroporation is possibly due to the enhanced poration at the trap aperture. The shielding of the cell membrane from the electric field by the PDMS microtrap reduces the poration away from the trap, causing improved cell viability during and after the microtrap electroporation procedure.

3.4. *Plasmid DNA electrotransfer in microtrap array induce efficient gene transfection*

Our geometry's high local electric fields lead to enhanced delivery of charged macromolecules such as DNA (negatively charged) to the cells. We hypothesize that this leads to better transfection at voltage conditions which do not cause a loss in cell viability. To test this, we deliver plasmid DNA (pEGFP-C1) encoding a green fluorescent protein (GFP) to CHO-K1 cells at two voltage conditions at which the single cells are permeabilized (90 V, 120 V, ten pulses of 5 ms each at 1 Hz) and one voltage condition at which the single cells are not permeabilized (60 V, ten pulses of 5 ms each at 1 Hz) in the microtrap device. As a negative control, we electroporate cells in the microtrap array without the plasmid DNA (120 V, ten pulses of 5 ms each at 1 Hz). Fig. 4(a), (b) show that upon electroporation of the CHO cells in the presence of the pEGFP-

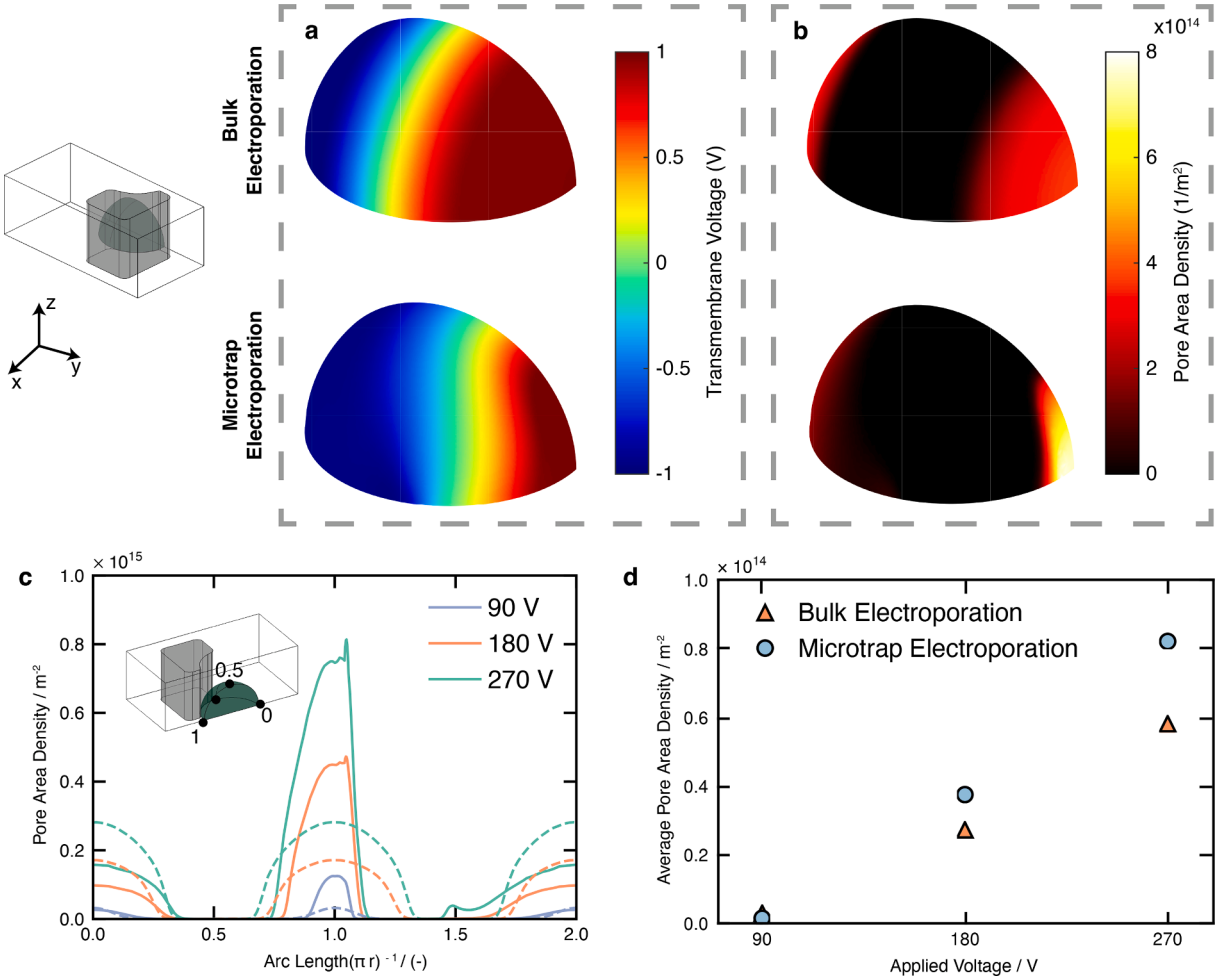

Fig. 3. Numerical simulations of electroporation in bulk and microtrap array. The orientation of the cell in the displayed results is shown. (a) The induced transmembrane voltage in bulk electroporation (top) and microtrap electroporation (bottom) shows that the microtrap alters the induced transmembrane voltage. (b) Pore area density in bulk electroporation (top) and microtrap electroporation (bottom) demonstrate localized electroporation near the microtrap aperture. These results correspond to an applied voltage drop of 270 V across the electrodes in the experiments. (c) Pore area density is plotted against the arc length normalized by πr. As shown in the inset, 0 in the variable shown in the *x*-axis corresponds to the point in the cell membrane on the side opposite to the microtrap aperture, 1 to the point in the cell membrane on the side of trap aperture. The voltages shown in the legend correspond to the voltage drop across the electrodes in the experiments. The solid lines correspond to microtrap electroporation while the dashed lines represent equivalent bulk electroporation. (d) Surface average pore area density on the simulated cell surface for different applied voltages for bulk electroporation and microtrap electroporation.

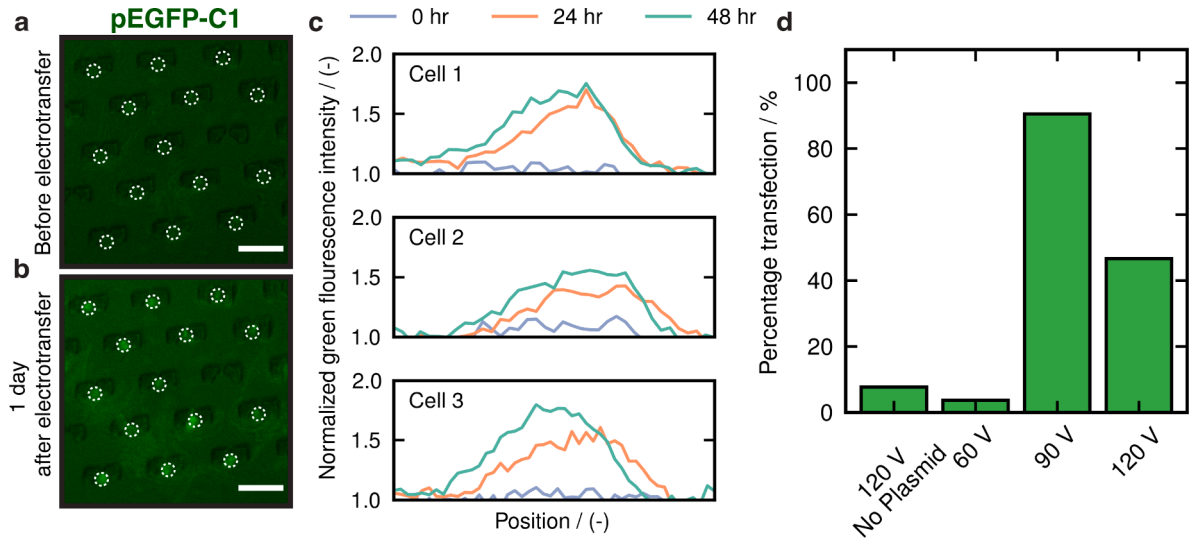

Fig. 4. GFP expression in microtrap array electroporation device using pEGFP-C1 plasmid DNA. (a), (b) Fluorescence microscopy images of the microtrap array with trapped cells (highlighted by dotted white circles) (a) before electrotransfer (b) one day after electrotransfer. The images shown are from experiment where 10 pulses of 90 V, each 5 ms long were applied. (c) Three representative examples of increase in green fluorescence intensity across of the cross section of cell after electrotransfer of pEGFP-C1 plasmids are presented. The fluorescence intensity is measured at three time points, 0 h (immediately after electrotransfer), 24 h and 48 h after electrotransfer. These cells are from the experiment with an applied voltage difference of 90 V. The fluorescence intensity is normalized by the fluorescence intensity at time $= 0$ h. (d) Percentage of cells showing transfection at different applied voltage conditions (120 V with no plasmid, 60 V, 90 V and 120 V, 10 pulses of 5 ms each) 24 day hours electrotransfer. Scale bar is 50 μm.

C1 plasmid DNA, cells display an enhanced green fluorescence for an applied voltage condition of 90 V. We measure the fluorescence intensity inside the cells at different time points in Fiji by manually selecting a region of interest that outlines the boundary of the cells (the region of interest are chosen in the first frame based on the Calcein Red channel used to stain the cells). Random shifts in the location of the cells during the time series imaging are manually corrected in Fiji. We observe $\sim$ 30% increase in green fluorescence intensity of the cells after one day for an applied voltage of 90 V and 120 V in the microtrap electroporation device (supplementary information, Fig. S13). To avoid photobleaching and phototoxicity, we use short exposure times, and to get as many cells as possible within the same frame, we use a low magnification ($10\times$). We believe these effects lead to the low increase in fluorescence intensity that we observe. We confirm that the increase in the fluorescence intensity is more than that of changes in the background fluorescence intensity after evaluating the background fluorescence intensity in randomly selected cell-sized regions of interest (see supplementary information, Fig. S13). We plot the fluorescence intensity (normalized by the fluorescence intensity at time $= 0$ h) across three representative cells (across the cell diameter) before electroporation, one day and two days after electroporation in the microtrap array in Fig. 4(c). Fig. 4(c) shows that the cells display a markedly higher fluorescence than the background fluorescence intensity. We then quantify the percentage transfection based on the percentage of cells that show a 20% increase in the green fluorescence intensity (only cells that show a 20% increase in fluorescence intensity and more than that of the background level increase are considered as transfected cells). We show in Fig. 4(d) that $>$ 90% of cells express green fluorescent protein at the applied voltage of 90 V within 24 h. For the applied voltage of 120 V, $\sim$ 45% are transfected, while for 60 V, only $\sim$ 3% cells display an increase in fluorescence intensity after electroporation in the presence of the pEGFP-C1 plasmids. In the negative control performed at 120 V in the absence of plasmid DNA, $\sim$ 7% cells show a 20% increase in green fluorescence intensity.

In contrast to small molecules such as propidium iodide, larger charged plasmid DNA first forms DNA-membrane complexes upon electrotransfer and is later internalized through cellular machinery [51–54]. Since the intracellular release of plasmid DNA is difficult to control without the use of endosomal/nuclear disrupting or redirecting agents [55–57], the amount of plasmid DNA that forms the DNA membrane complex and the cell viability is key to successful cell transfection [58,59]. We believe the high local electric fields cause electrophoretic drift of large amounts of plasmid DNA towards the cell membrane upon application of electric pulses. Furthermore, as demonstrated in the previous sections, our device provides improved cell viability. The combination of a high local concentration of plasmid DNA and good cell viability allows the device to transfect the cells successfully.

4. Conclusions

A microfluidic device that enables localized electroporation in a microtrap array is presented. The simple working mechanism of the device allows the positioning of the cell to locations with high local electric fields by the flow. The device is compatible with delivering membrane-impermeable small molecules such as fluorescent tracer molecules and larger charged molecules such as plasmid DNA. Electroporation in this device enables the transfer of molecules while preserving cell viability. A high degree of gene transfection is obtained when protein-encoding plasmid DNA is electrotransferred with this device. The micro trap electroporation device demonstrated here is expected to open up the possibility for a robust localized electroporation procedure (with perfect cell viability and uniformity) in gene therapy, *ex vivo* applications (based on adoptive immunotherapy), and drug delivery applications.

Author contributions

A.M. and P.E.B. conceptualized and supervised the research. A.M. and G.R.P. developed the methodology. A.M., G.R.P., and L.R. performed the research with inputs from H.H. (microfluidics fabrication) and M.N-G. (scanning electron microscopy). A.M. wrote the manuscript with inputs from all the authors. Finally A.M., P.E.B., G.R.P. and L.R. revised and finalised the paper.

Declaration of Competing Interest

The authors declare that they have no known competing financial interests or personal relationships that could have appeared to influence the work reported in this paper.

Acknowledgements

The authors thank Peter ten Dijke (Leiden University Medical Center) for providing the pEGFP-C1 plasmids used in this research. The research performed in this article was supported by the funding from the European Research Council under the European Union's Horizon 2020 research and innovation programme (grant agreement No. 819424). G. R.P. was supported by the funding from the German Research Foundation (Deutsche Forschungsgemeinschaft, DFG) through a postdoctoral research fellowship (PE 3015/2–1).

Appendix A. Supplementary material

Supplementary data associated with this article can be found, in the online version, at https://doi.org/10.1016/j.bioelechem.2022.108197.

References

[1] M.R. Prausnitz, V.G. Bose, R. Langer, J.C. Weaver, Electroporation of mammalian skin: a mechanism to enhance transdermal drug delivery, Proc. Nat. Acad. Sci. 90 (22) (1993) 10504–10508, https://doi.org/10.1073/pnas.90.22.10504.
[2] L.M. Mir, M.F. Bureau, J. Gehl, R. Rangara, D. Rouy, J.-M. Caillaud, P. Delaere, D. Branellec, B. Schwartz, D. Scherman, High-efficiency gene transfer into skeletal muscle mediated by electric pulses, Proc. Nat. Acad. Sci. 96 (8) (1999) 4262–4267, https://doi.org/10.1073/pnas.96.8.4262.
[3] M.L. Yarmush, A. Golberg, G. Serša, T. Kotnik, D. Miklavčič, Electroporation-based technologies for medicine: principles, applications, and challenges, Annu. Rev. Biomed. Eng. 16 (2014) 295–320, https://doi.org/10.1146/annurev-bioeng-071813-104622.
[4] W. Kang, R.L. McNaughton, H.D. Espinosa, Micro-and nanoscale technologies for delivery into adherent cells, Trends Biotechnol. 34 (8) (2016) 665–678, https://doi.org/10.1016/j.tibtech.2016.05.003.
[5] M.P. Stewart, R. Langer, K.F. Jensen, Intracellular delivery by membrane disruption: mechanisms, strategies, and concepts, Chem. Rev. 118 (16) (2018) 7409–7531, https://doi.org/10.1021/acs.chemrev.7b00678.
[6] J. Brooks, G. Minnick, P. Mukherjee, A. Jaberi, L. Chang, H.D. Espinosa, R. Yang, High throughput and highly controllable methods for in vitro intracellular delivery, Small 16 (51) (2020) 2004917, https://doi.org/10.1002/smll.202004917.
[7] P.J. Canatella, J.F. Karr, J.A. Petros, M.R. Prausnitz, Quantitative study of electroporation-mediated molecular uptake and cell viability, Biophys. J . 80 (2) (2001) 755–764, https://doi.org/10.1016/S0006-3495(01)76055-9.
[8] S. Sachdev, T. Potočnik, L. Rems, D. Miklavčič, Revisiting the role of pulsed electric fields in overcoming the barriers to in vivo gene electrotransfer, Bioelectrochemistry 107994 (2021), https://doi.org/10.1016/j.bioelechem.2021.107994.
[9] P.E. Boukany, A. Morss, W.-C. Liao, B. Henslee, H. Jung, X. Zhang, B. Yu, X. Wang, Y. Wu, L. Li, et al., Nanochannel electroporation delivers precise amounts of biomolecules into living cells, Nat. Nanotechnol. 6 (11) (2011) 747–754, https://doi.org/10.1038/nnano.2011.164.
[10] Y. Cao, E. Ma, S. Cestellos-Blanco, B. Zhang, R. Qiu, Y. Su, J.A. Doudna, P. Yang, Nontoxic nanopore electroporation for effective intracellular delivery of biological macromolecules, Proc. Nat. Acad. Sci. 116 (16) (2019) 7899–7904, https://doi.org/10.1073/pnas.1818553116.
[11] S. Wang, L.J. Lee, Micro-/nanofluidics based cell electroporation, Biomicrofluidics 7 (1) (2013) 011301, https://doi.org/10.1063/1.4774071.
[12] L. Rems, D. Kawale, L.J. Lee, P.E. Boukany, Flow of DNA in micro/nanofluidics: From fundamentals to applications, Biomicrofluidics 10 (4) (2016) 043403, https://doi.org/10.1063/1.4958719.
[13] M. Khine, A. Lau, C. Ionescu-Zanetti, J. Seo, L.P. Lee, A single cell electroporation chip, Lab Chip 5 (1) (2005) 38–43, https://doi.org/10.1039/b408352k.
[14] H. Lu, M.A. Schmidt, K.F. Jensen, A microfluidic electroporation device for cell lysis, Lab Chip 5 (1) (2005) 23–29, https://doi.org/10.1039/B406205A.
[15] K. Gao, L. Li, L. He, K. Hinkle, Y. Wu, J. Ma, L. Chang, X. Zhao, D.G. Perez, S. Eckardt, et al., Design of a microchannel-nanochannel-microchannel array based nanoelectroporation system for precise gene transfection, Small 10 (5) (2014) 1015–1023, https://doi.org/10.1002/smll.201300116.
[16] L. Chang, M. Howdyshell, W.-C. Liao, C.-L. Chiang, D. Gallego-Perez, Z. Yang, W. Lu, J.C. Byrd, N. Muthusamy, L.J. Lee, et al., Magnetic tweezers-based 3D microchannel electroporation for high-throughput gene transfection in living cells, Small 11 (15) (2015) 1818–1828, https://doi.org/10.1002/smll.201402564.
[17] L. Chang, D. Gallego-Perez, X. Zhao, P. Bertani, Z. Yang, C.-L. Chiang, V. Malkoc, J. Shi, C.K. Sen, L. Odonnell, et al., Dielectrophoresis-assisted 3D nanoelectroporation for non-viral cell transfection in adoptive immunotherapy, Lab Chip 15 (15) (2015) 3147–3153, https://doi.org/10.1039/C5LC00553A.
[18] L. Chang, D. Gallego-Perez, C.-L. Chiang, P. Bertani, T. Kuang, Y. Sheng, F. Chen, Z. Chen, J. Shi, H. Yang, et al., Controllable large-scale transfection of primary mammalian cardiomyocytes on a nanochannel array platform, Small 12 (43) (2016) 5971–5980, https://doi.org/10.1002/smll.201601465.
[19] D. Gallego-Perez, L. Chang, J. Shi, J. Ma, S.-H. Kim, X. Zhao, V. Malkoc, X. Wang, M. Minata, K.J. Kwak, et al., On-chip clonal analysis of glioma-stem-cell motility and therapy resistance, Nano Lett. 16 (9) (2016) 5326–5332, https://doi.org/10.1021/acs.nanolett.6b00902.
[20] L. Chang, P. Bertani, D. Gallego-Perez, Z. Yang, F. Chen, C. Chiang, V. Malkoc, T. Kuang, K. Gao, L.J. Lee, et al., 3D nanochannel electroporation for high-throughput cell transfection with high uniformity and dosage control, Nanoscale 8 (1) (2016) 243–252, https://doi.org/10.1039/C5NR03187G.
[21] D. Gallego-Pérez, D. Pal, S. Ghatak, V. Malkoc, N. Higuita-Castro, S. Gnyawali, L. Chang, W.-C. Liao, J. Shi, M. Sinha, et al., Topical tissue nano-transfection mediates non-viral stroma reprogramming and rescue, Nat. Nanotechnol. 12 (10) (2017) 974–979, https://doi.org/10.1038/nnano.2017.134.
[22] P. Mukherjee, S.S.P. Nathamgari, J.A. Kessler, H.D. Espinosa, Combined numerical and experimental investigation of localized electroporation-based cell transfection and sampling, ACS Nano 12 (12) (2018) 12118–12128, https://doi.org/10.1021/acsnano.8b05473.
[23] Z. Yang, J. Shi, J. Xie, Y. Wang, J. Sun, T. Liu, Y. Zhao, X. Zhao, X. Wang, Y. Ma, et al., Large-scale generation of functional mRNA-encapsulating exosomes via cellular nanoporation, Nat. Biomed. Eng. 4 (1) (2020) 69–83, https://doi.org/10.1038/s41551-019-0485-1.
[24] Z. Fei, S. Wang, Y. Xie, B.E. Henslee, C.G. Koh, L.J. Lee, Gene transfection of mammalian cells using membrane sandwich electroporation, Anal. Chem. 79 (15) (2007) 5719–5722, https://doi.org/10.1021/ac070482y.
[25] X. Xie, A.M. Xu, S. Leal-Ortiz, Y. Cao, C.C. Garner, N.A. Melosh, Nanostraw–electroporation system for highly efficient intracellular delivery and transfection, ACS Nano 7 (5) (2013) 4351–4358, https://doi.org/10.1021/nn400874a.
[26] Y. Cao, H. Chen, R. Qiu, M. Hanna, E. Ma, M. Hjort, A. Zhang, R. Lewis, J. Wu, N. Melosh, Universal intracellular biomolecule delivery with precise dosage control, Sci. Adv. 4 (10) (2018) eaat8131, https://doi.org/10.1126/sciadv.aat8131.
[27] G. He, J. Feng, A. Zhang, L. Zhou, R. Wen, J. Wu, C. Yang, J. Yang, C. Li, D. Chen, et al., Multifunctional branched nanostraw-electroporation platform for intracellular regulation and monitoring of circulating tumor cells, Nano Lett. 19 (10) (2019) 7201–7209, https://doi.org/10.1021/acs.nanolett.9b02790.
[28] X. Liu, A.-Y. Chang, Y. Ma, L. Hua, Z. Yang, S. Wang, Robust three-dimensional nanotube-in-micropillar array electrodes to facilitate size independent electroporation in blood cell therapy, Lab Chip (2021), https://doi.org/10.1039/D1LC00690H.
[29] W. Kang, F. Yavari, M. Minary-Jolandan, J.P. Giraldo-Vela, A. Safi, R. L. McNaughton, V. Parpoil, H.D. Espinosa, Nanofountain probe electroporation (NFP-E) of single cells, Nano Lett. 13 (6) (2013) 2448–2457, https://doi.org/10.1021/nl400423c.
[30] R. Yang, V. Lemaître, C. Huang, A. Haddadi, R. McNaughton, H.D. Espinosa, Monoclonal cell line generation and CRISPR/Cas9 manipulation via single-cell electroporation, Small 14 (12) (2018) 1702495, https://doi.org/10.1002/smll.201702495.
[31] S.S.P. Nathamgari, N. Pathak, V. Lemaitre, P. Mukherjee, J.J. Muldoon, C.-Y. Peng, T. McGuire, J.N. Leonard, J.A. Kessler, H.D. Espinosa, Nanofountain probe electroporation enables versatile single-cell intracellular delivery and investigation of postpulse electropore dynamics, Small 16 (43) (2020) 2002616, https://doi.org/10.1002/smll.202002616.
[32] S.-O. Choi, Y.-C. Kim, J.W. Lee, J.-H. Park, M.R. Prausnitz, M.G. Allen, Intracellular protein delivery and gene transfection by electroporation using a microneedle electrode array, Small 8 (7) (2012) 1081–1091, https://doi.org/10.1002/smll.201101747.
[33] D. Xia, R. Jin, G. Byagathvalli, H. Yu, L. Ye, C.-Y. Lu, M.S. Bhamla, C. Yang, M. R. Prausnitz, An ultra-low-cost electroporator with microneedle electrodes (ePatch) for SARS-CoV-2 vaccination, Proc. Nat. Acad. Sci. 118 (45) (2021), https://doi.org/10.1073/pnas.211081711.
[34] Y. Xuan, S. Ghatak, A. Clark, Z. Li, S. Khanna, D. Pak, M. Agarwal, S. Roy, P. Duda, C.K. Sen, Fabrication and use of silicon hollow-needle arrays to achieve tissue nanotransfection in mouse tissue in vivo, Nat. Protoc. (2021) 1–32, https://doi.org/10.1038/s41596-021-00631-0.
[35] X. Zhao, X. Huang, X. Wang, Y. Wu, A.-K. Eisfeld, S. Schwind, D. Gallego-Perez, P. E. Boukany, G.I. Marcucci, L.J. Lee, Nanochannel electroporation as a platform for living cell interrogation in acute myeloid leukemia, Adv. Sci. 2 (12) (2015) 1500111, https://doi.org/10.1002/advs.201500111.
[36] P.E. Boukany, Y. Wu, X. Zhao, K.J. Kwak, P.J. Glazer, K. Leong, L.J. Lee, Nonendocytic delivery of lipoplex nanoparticles into living cells using nanochannel electroporation, Adv. Healthc. Mater. 3 (5) (2014) 682–689, https://doi.org/10.1002/adhm.201300213.
[37] K. Gao, X. Huang, C.-L. Chiang, X. Wang, L. Chang, P. Boukany, G. Marcucci, R. Lee, L.J. Lee, Induced apoptosis investigation in wild-type and FLT3-ITD acute myeloid leukemia cells by nanochannel electroporation and single-cell qRT-PCR, Mol. Ther. 24 (5) (2016) 956–964, https://doi.org/10.1038/mt.2016.6.
[38] A. Huebner, D. Bratton, G. Whyte, M. Yang, A.J. Demello, C. Abell, F. Hollfelder, Static microdroplet arrays: a microfluidic device for droplet trapping, incubation and release for enzymatic and cell-based assays, Lab Chip 9 (5) (2009) 692–698, https://doi.org/10.1039/B813709A.

[39] Y. Kazayama, T. Teshima, T. Osaki, S. Takeuchi, T. Toyota, Integrated microfluidic system for size-based selection and trapping of giant vesicles, Anal. Chem. 88 (2) (2016) 1111–1116, https://doi.org/10.1021/acs.analchem.5b03772.
[40] Y. Xia, G.M. Whitesides, Soft lithography, Annu. Rev. Mater. Sci. 28 (1) (1998) 153–184, https://doi.org/10.1146/annurev.matsci.28.1.153.
[41] L. Retelj, G. Pucihar, D. Miklavčič, Electroporation of intracellular liposomes using nanosecond electric pulses—a theoretical study, IEEE Trans. Biomed. Eng. 60 (9) (2013) 2624–2635, https://doi.org/10.1109/TBME.2013.2262177.
[42] J.C. Neu, W. Krassowska, Asymptotic model of electroporation, Phys. Rev. E 59 (3) (1999) 3471, https://doi.org/10.1103/PhysRevE.59.3471.
[43] K.A. DeBruin, W. Krassowska, Modeling electroporation in a single cell. I. Effects of field strength and rest potential, Biophys. J . 77 (3) (1999) 1213–1224, https://doi.org/10.1016/S0006-3495(99)76973-0.
[44] W. Krassowska, P.D. Filev, Modeling electroporation in a single cell, Biophys. J . 92 (2) (2007) 404–417, https://doi.org/10.1529/biophysj.106.094235.
[45] J. Li, W. Tan, M. Yu, H. Lin, The effect of extracellular conductivity on electroporation-mediated molecular delivery, Biochim. Biophys. Acta (BBA) - Biomembr. 1828 (2) (2013) 461–470, https://doi.org/10.1016/j.bbamem.2012.08.014.
[46] G. Pucihar, T. Kotnik, D. Miklavčič, J. Teissié, Kinetics of transmembrane transport of small molecules into electropermeabilized cells, Biophys. J . 95 (6) (2008) 2837–2848, https://doi.org/10.1529/biophysj.108.135541.
[47] T.B. Napotnik, D. Miklavčič, In vitro electroporation detection methods–an overview, Bioelectrochemistry 120 (2018) 166–182, https://doi.org/10.1016/j.bioelechem.2017.12.005.
[48] A. Muralidharan, L. Rems, M.T. Kreutzer, P.E. Boukany, Actin networks regulate the cell membrane permeability during electroporation, Biochim. Biophys. Acta (BBA) - Biomembr. 1863 (1) (2021) 183468, https://doi.org/10.1016/j.bbamem.2020.183468.
[49] Z. Fan, H. Liu, M. Mayer, C.X. Deng, Spatiotemporally controlled single cell sonoporation, Proc. Nat. Acad. Sci. 109 (41) (2012) 16486–16491, https://doi.org/10.1073/pnas.1208198109.
[50] T. Kotnik, G. Pucihar, D. Miklavčič, The cell in the electric field, in: Clinical Aspects of Electroporation, Springer, 2011, pp. 19–29. https://link.springer.com/chapter/10.1007/978-1-4419-8363-3_3.
[51] M. Golzio, J. Teissié, M.-P. Rols, Direct visualization at the single-cell level of electrically mediated gene delivery, Proc. Nat. Acad. Sci. 99 (3) (2002) 1292–1297, https://doi.org/10.1073/pnas.022646499.
[52] C. Rosazza, A. Buntz, T. Rieß, D. Wöll, A. Zumbusch, M.-P. Rols, Intracellular tracking of single-plasmid DNA particles after delivery by electroporation, Mol. Ther. 21 (12) (2013) 2217–2226.
[53] C. Rosazza, S. Haberl Meglic, A. Zumbusch, M.-P. Rols, D. Miklavcic, Gene electrotransfer: a mechanistic perspective, Curr. Gene Ther. 16 (2) (2016) 98–129, https://doi.org/10.2174/1566523216666160331130040.
[54] A. Muralidharan, H. Uitenbroek, P.E. Boukany, Intracellular transport of electrotransferred DNA cargo is governed by coexisting ergodic and non ergodic anomalous diffusion, bioRxiv (2021), https://doi.org/10.1101/2021.04.12.435513.
[55] X. Ding, M.P. Stewart, A. Sharei, J.C. Weaver, R.S. Langer, K.F. Jensen, High-throughput nuclear delivery and rapid expression of DNA via mechanical and electrical cell-membrane disruption, Nat. Biomed. Eng. 1 (3) (2017) 1–7, https://doi.org/10.1038/s41551-017-0039.
[56] L.D. Cervia, C.-C. Chang, L. Wang, M. Mao, F. Yuan, Enhancing electrotransfection efficiency through improvement in nuclear entry of plasmid DNA, Mol. Therapy-Nucl. Acids 11 (2018) 263–271, https://doi.org/10.1016/j.omtn.2018.02.009.
[57] M. Mao, C.-C. Chang, A. Pickar-Oliver, L.D. Cervia, L. Wang, J. Ji, P.B. Liton, C. A. Gersbach, F. Yuan, Redirecting vesicular transport to improve nonviral delivery of molecular cargo, Adv. Biosyst. 4 (8) (2020) 2000059, https://doi.org/10.1002/adbi.202000059.
[58] C. Faurie, M. Rebersek, M. Golzio, M. Kanduser, J.-M. Escoffre, M. Pavlin, J. Teissie, D. Miklavcic, M.-P. Rols, Electro-mediated gene transfer and expression are controlled by the life-time of DNA/membrane complex formation, J. Gene Med. 12 (1) (2010) 117–125, https://doi.org/10.1002/jgm.1414.
[59] J.-M. Escoffre, T. Portet, C. Favard, J. Teissié, D.S. Dean, M.-P. Rols, Electromediated formation of DNA complexes with cell membranes and its consequences for gene delivery, Biochim. Biophys. Acta (BBA)-Biomembr. 1808 (6) (2011) 1538–1543, https://doi.org/10.1016/j.bbamem.2010.10.009.